Wavelength selective colloidal quantum dot photodetecors for spectral analysis

Carlo Venettacci[1], Andrea De Iacovo[1*], Federica Mitri[1], Carlo Giansante[2], Lorenzo Colace[1]
1: Department of Engineering, University Roma Tre, Via Vito Volterra 62, 00146, Rome, Italy
2: CNR Nanotec, Istituto di Nanotecnologia, Via Monteroni, Lecce 73100, Italy
*: andrea.deiacovo@uniroma3.it

***Abstract*—Colloidal quantum dots attracted much attention for the development of optoelectronic devices thanks to their tunable optical and electronic properties. In this work we report on wavelength selective photodetectors based on colloidal quantum dots operating in the visible and near infrared spectral range. We demonstrate that arrays of such devices, along with processing algorithms, are suitable for the detection of spectral features of the measured optical radiation.**

Keywords—Colloidal Quantum Dots; Photodetectors, wavelength-selective devices;

I. Introduction

Colloidal quantum dots (QD) are solution processed semiconductor nanoparticles that exhibit unique optical properties such as large optical absorption and emission and size tunability [1]. In addition, surface chemistry, through ligand exchange procedures can be performed to further change their properties [2]. Their rapid development is also due to their ease of synthesis and fabrication and their compatibility with several substrates, including silicon. For such reasons, QD have been successfully employed for the fabrication of several devices, including light emitting diodes, lasers, optical modulators, solar cells, and photodetectors [3].
QD size tunability has been generally used to select the spectral range of interest, according to the targeted application. Here we exploit the size tunability for the fabrication of sets of narrowband photodetectors with different spectral responses to be used for the measurement of the spectral features of an optical radiation.
In recent years, wavelength selective and spectrally tunable photodetectors in the visible (Vis) and near infrared (NIR) have been proposed, resorting to both QD filters and/or QD photodetectors [4,5]. Following the first demonstration of QD narrowband photodetectors [6], we have previously proposed an approach based on the employment of an array of QD photodetectors provided with QD filters, with different absorption characteristics, for the the identification of the peak wavelength of a quasi-monochromatic optical radiation [7]. Here, we increase the set of QD narrowband tunable photodetectors and develop new algorithms for more complex spectral analysis.

II. Device Fabrication

PbS QD have been synthesized using a slightly modified, well-established wet chemistry technique [8]. Reagents were injected into a three-neck flask connected to a standard Schlenk line setup and nanocrystals of different sizes have been fabricated controlling the reagent concentrations, temperature, reaction times and ligand selection. The synthesis is followed by isolation and redispersion in toluene for subsequent solution processing. More details on the synthesis can be found elsewhere [9].
Seven QD dispersion were synthesized with QD diameter ranging from 2 to 5 nm (2.0, 2.7, 3.2, 4.2, 4.5, 4.7, 5 nm).
Photoconductors were fabricated by spin-coating PbS QD dispersions on interdigitated gold contacts, with 1 mm^2 area and 5 µm finger spacing on a SiO_2/Si substrate. The procedure consists of a layer-by-layer technique, which alternates the QD deposition with the rinsing of the device in a 10 mg ml^{-1} tetrabutylammonium iodide (TBAI) methanol solution to replace the original, electrically insulating oleate inter dot ligands with shorter I^- anions, providing the desired transport properties and QD passivation [10]. The process was repeated ten times, to achieve a suitable thickness. Finally, photoconductors were thermally annealed at 100°C for one hour. The same QD dispersions were also employed for the realization of optical filters by drop-casting onto planar glass substrates, without ligand exchange or thermal annealing procedure.
Narrowband detectors have been obtained stacking the photoconductors with QD filters as schematically shown in fig.1.

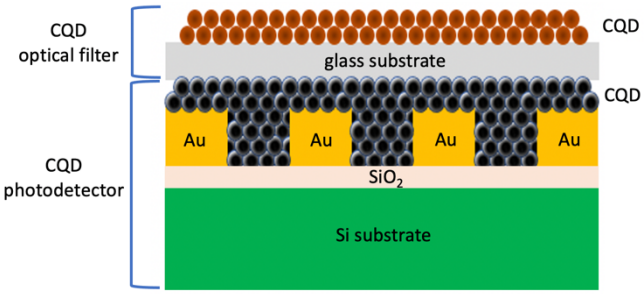

Fig. 1. Schematic cross-section of the narrowband photoconductors made of two functional PbS QD layers (optical filter and photodetector).

A typical example of the narrowed spectral response is shown in Fig. 2, where an unfiltered photodetector responsivity, a QD-on-glass filter absorbance and the resulting photoresponse of the filtered device are reported. The optoelectronic characterization in terms of dark current, responsivity and detectivity has been reported in previous works [11].

III. Photodetector Data Set

Combining different filters and detectors from the available dispersions, we obtained a large set of narrowband photodetectors spanning over the whole Vis-NIR range. Selecting the narrowest shifted spectral responses, we

obtained the set reported in Fig.3 where seven photodetectors, spanning the near infrared range, are shown.
Such an array of photodetectors could be directly employed as a 7-channel detector operating in the near infrared.

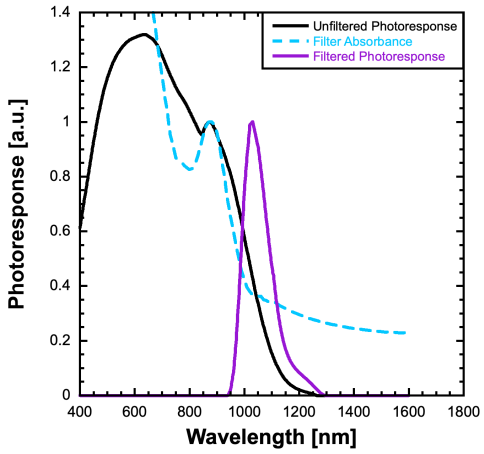

Fig. 2. Unfiltered (black line) and filtered (purple line) photodetector response spectrum. Filter absorbance is showed in blue.

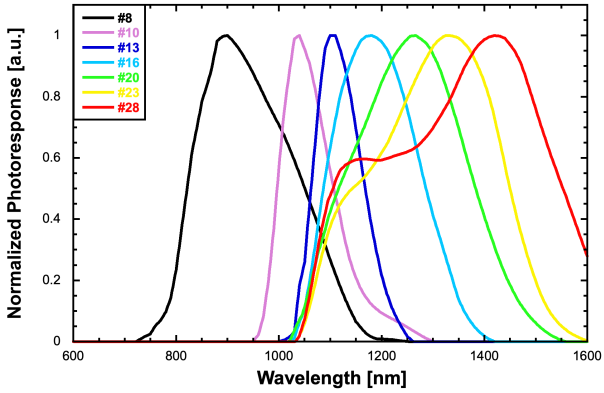

Fig. 3. Spectral response of selected narrowband photodetectors.

The combination of all photodetectors with all optical filters produced a very large set of spectral responses. However, some of them turned out to be quite similar. After a selection based on getting the largest number of spectral responses exhibiting different features, we ended up with a set of 28 devices. The QD dimension used for the photodetectors (d) and for the optical filters (d_{filt}) and their combination are reported in Table I, while the corresponding spectral responses are shown in Fig.4.

#	d	d_{filt}	#	d	d_{filt}
1	2.0	N.A.	8	2.0	2.0
2	2.7	N.A.	9	2.7	2.0
3	3.2	N.A.	10	2.7	2.7
4	4.2	N.A.	11	3.2	2.0
5	4.5	N.A.	12	3.2	2.7
6	4.7	N.A.	13	3.2	3.2
7	5.0	N.A.	14	4.2	2.0
15	4.2	2.7	22	4.7	2.7
16	4.2	3.2	23	4.7	3.2
17	4.2	4.2	24	4.7	4.2
18	4.5	2.0	25	4.7	4.7
19	4.5	2.7	26	5.0	2.0
20	4.5	3.2	27	5.0	2.7
21	4.7	2.0	28	5.0	3.2

Table I: QD used for the 28 photodetectors shown in Fig.4. d and d_{filt} are the QD dimension in nanometers for the photoconductor and the optical filter, respectively.

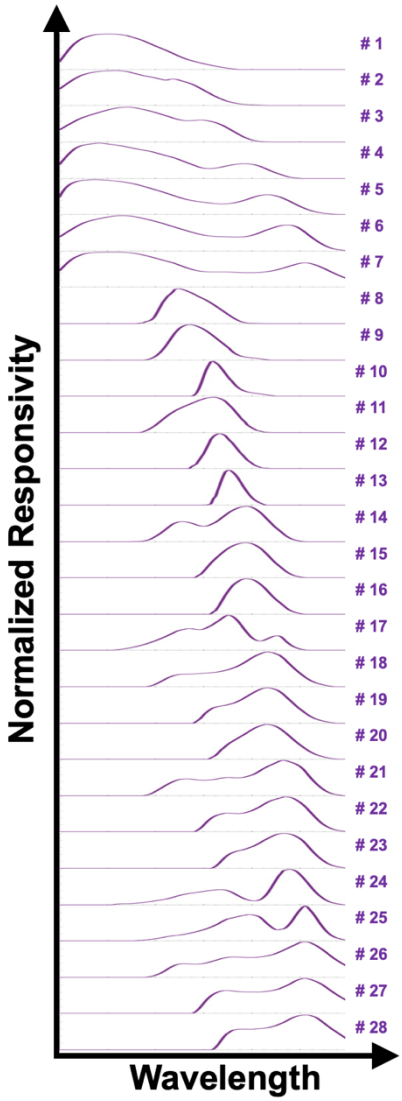

Fig. 4. Device responsivity data set in the 400–1600 nm range. The absorption spectra in the first seven rows are from unfiltered photoconductors. Rows 8–28 are referred to different combinations of photodetectors and QD optical filters, resulting in an effective narrowing or significant modification of the spectral response.

Here we demonstrate that this large set of photoresponses can be combined with suitable algorithms for the extraction of the peak wavelength of a quasi-monochromatic radiation and the reconstruction of the emission spectrum of an unknown light source, in the Vis-NIR range.
If an optical radiation with power spectrum P(λ) reaches the different photodetectors and each device is characterized by a responsivity spectrum $R_n(\lambda)$ (such as the ones shown in fig. 4), then a set of photocurrents can be measured, each one defined according to eq. 1, where λ_{min} and λ_{max} are the minimum and maximum wavelengths where $R_n(\lambda) = 0$, and the subscript n refers to a specific photodetector within the fabricated set.

$$i_n = \int_{\lambda_{min}}^{\lambda_{max}} R_n(\lambda) P(\lambda) \delta\lambda \qquad (1)$$

Assuming that both R(λ) and P(λ) can be measured with a finite wavelength accuracy, and that all the photodetectors are illuminated with the same P(λ), eq. 1 can be rewritten in matrix form as in eq. 2, where $\bar{\bar{R}}$ is an n x m matrix (with n and m being the number of photodetectors and measured

wavalengths, respectively) and $\bar{P}$ is a column vector with length m.

$$\bar{\iota} = \bar{\bar{R}} \times \bar{P} \qquad (2)$$

The power spectrum of the optical radiation can be calculated solving the linear equation system described by eq. 2. In order to do so, we need to calculate the inverse matrix $\bar{\bar{R}}^{-1}$. $\bar{\bar{R}}$ may not be square and its rank may be lower than n, thus $\bar{\bar{R}}^{-1}$ cannot be directly calculated in a closed form. For this reason, we calculated it numerically, with a classic Levenberg-Marquardt fitting algorithm. We calculated $\bar{\bar{R}}^{-1}$ so that:

$$\bar{\bar{Q}} = \bar{\bar{R}}^{-1} \times \bar{\bar{R}} \qquad (3)$$

where $\bar{\bar{Q}}$ is a m x m matrix. The fit was executed constraining each row of $\bar{\bar{Q}}$ according to eq. 4, where m_0 represents a wavelength and ranges from 400nm to 1600nm, ad σ is an optimization parameter.

$$\bar{Q}_n = e^{\frac{(m-m_0)^2}{\sigma^2}} \qquad (4)$$

IV. Results and Discussion

The first application of the proposed system is a wavemeter for quasi monochromatic beams. In order to estimate the accuracy of the proposed system, we simulated the photocurrents produced by the photodetectors upon illumination with a quasi-monochromatic radiation with gaussian spectra with a 15 nm standard deviation and emission peaks evenly spaced in the 400–1600 nm spectral range. Fig. 5 shows the extracted wavelength peaks versus the theorical ones (top), and the local error in nm (bottom).

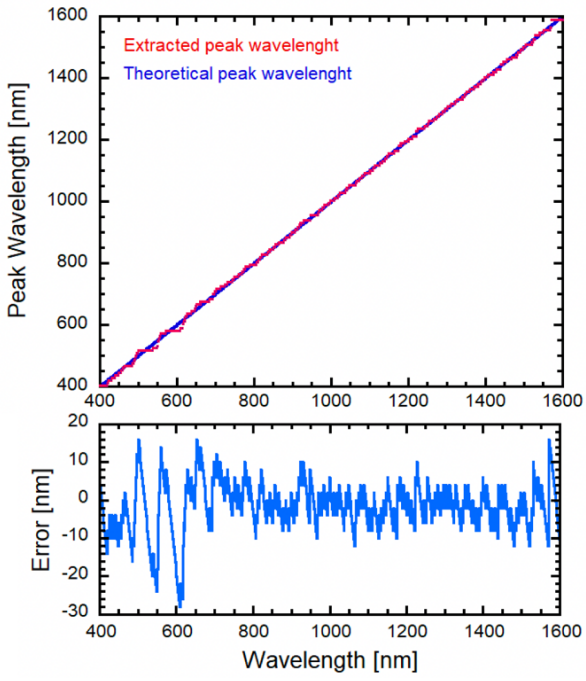

Fig. 5. Calculated peak wavelength vs theoretical peak (top) and local error (bottom).

A 0.3% mean error (corresponding to ±5 nm) has been obtained. The larger errors occur below 800 nm, reaching an absolute maximum error of 28 nm at 608 nm. For most of the NIR spectral range the maximum absolute error is within ±10nm. The mean error remained lower than 1% even reducing the number of photodetectors to ten, carefully choosing the devices with evenly spaced responsivity peaks over the vis-NIR spectrum. The peak wavelength identification system represents a simplified application of the spectrum reconstruction algorithm explained before. In fact, since we assumed the imping radiation being quasi-monochromatic, we didn't try to reconstruct the whole optical spectrum, but we simply identified the maximum power wavelength. In order to verify the robustness of the proposed system and its suitability as a spectrum analyzer, we also employed it for the reconstruction of a full vis-NIR spectrum. Fig. 6 reports an example of the reconstruction (red) of a complex source (black) simulated by a weighted superposition of gaussian beams of different bandwidth. The bottom of Fig. 6 showing the % error versus wavelength demonstrates the error is within ±10% in most of the Vis and NIR spectral range. We have investigated the system's capability reducing the number of detectors. The performance depends on the number of the devices employed; however, a set of ten selected devices allows a mean error of 5%, averaged over the entire spectrum between 400 and 1600 nm.

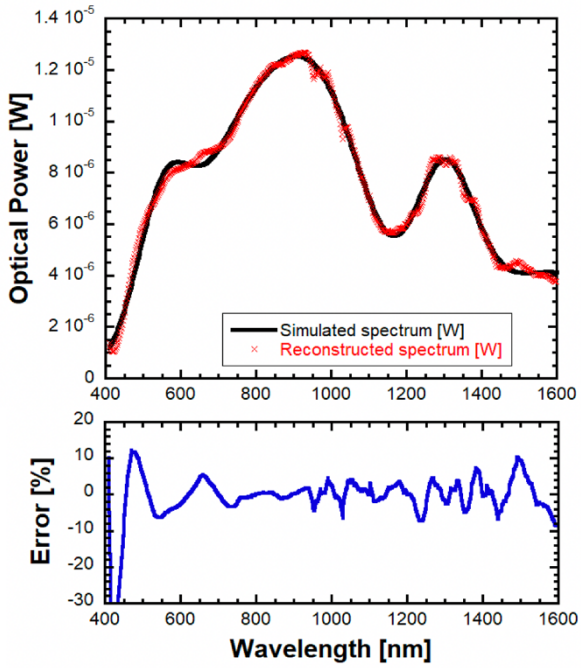

Fig. 6. Example of experimental reconstruction of broadband target sources (top) and corresponding local error (bottom).

V. Conclusions

In this work, we demonstrated that PbS CQD photodetectors can be engineered to obtain multichannel detectors operating in the Vis and NIR spectral range. In addition, a relatively small set of photodetectors with different engineered spectral responses can be combined with postprocessing procedures to be employed for spectral analysis such as the extraction of the peak wavelength of a quasi-monochromatic radiation, and the identification of the spectral components of a broad-band light source.

Acknowledgment

C. G. thanks Progetto di ricerca MIUR PON 2014-2020, Energia per l'Ambiente TARANTO (Project Number: ARS01_00637).

REFERENCES

[1] J.K. Kim, O. Voznyy, D. Zhitomirsky, E.H. Sargent, "Colloidal Quantum Dot Materials and Devices: A Quarter-Century of Advances" *Adv. Mater*., vol. 25, no. 36, pp. 4986-5010, Sep. 2013.

[2] P. R. Brown, D. Kim, R. R. Lunt, N. Zhao, M. G. Bawendi, J. C. Grossman, V. Bulovic, "Energy Level Modification in Lead Sulfide Quantum Dot Thin Films through Ligand Exchange" ACS Nano 2014, 8, 5863.

[3] C.R. Kagan, E. Lifshitz, E.H. Sargent, D.V. Talapin, "Building devices from colloidal quantum dots" *Science* , vol. 353, no. 6302, pp. 885-895, Aug. 2016.

[4] J. Bao, M.G. Bawendi, A colloidal quantum dot spectrometer, Nature 523 (2015) 67–70.

[5] Lin, Q.; Armin, A.; Burn, P. L.; Meredith, P. Filterless Narrowband Visible Photodetectors. *Nat. Photonics* **2015**, *9* (10), 687–694.

[6] K. Qiao, H. Deng, X. Yang, D. Dong, M. Li, L. Hu, et al., Spectra-selective PbS quantum dot infrared photodetectors, Nanoscale 8 (13) (2016) 7137-7143.

[7] A. De Iacovo, C. Venettacci, C. Giansante, L. Colace, Narrowband colloidal quantum dot photodetectors for wavelength measurement applications, Nanoscale 12 (18) (2020) 10044–10050.

[8] M.A. Hines, G.D. Scholes, Colloidal PbS nanocrystals with size-tunable near-infrared emission: observation of post- synthesis self-narrowing of the particle size distribution, Adv. Mater. 15 (21) (2003) 1844–1849.

[9] C. Giansante, Surface chemistry control of colloidal quantum dot band gap, J. Phys. Chem. C 122 (31) (2018) 18110−18116.

[10] I.D. Skurlov, I.G. Korzhenevskii, A.S. Mudrak, A. Dubavik, S.A. Cherevkov, P.S. Parfenov, X. Zhang, A.V. Fedorov, A.P. Litvin, and A.V. Baranov, Optical Properties, Morphology, and Stability of Iodide-Passivated Lead Sulfide Quantum Dots, Materials 12 (19) (2019).

[11] De Iacovo, A. Venettacci, C. Colace, L. Scopa, L. Foglia, S. Noise Performance of PbS Colloidal Quantum Dot Photodetectors. *Appl. Phys. Lett.* **2017**, *111* (21).